

AC-VRNN: Attentive Conditional-VRNN for Multi-Future Trajectory Prediction

Alessia Bertugli¹, Simone Calderara², Pasquale Coscia³, Lamberto Ballan³,
and Rita Cucchiara²

¹ University of Trento, Italy, name.surname@unitn.it

² University of Modena and Reggio Emilia, Italy, name.surname@unimore.it

³ University of Padova, Italy, name.surname@unipd.it

Abstract. Anticipating human motion in crowded scenarios is essential for developing intelligent transportation systems, social-aware robots and advanced video-surveillance applications. An important aspect of such task is represented by the inherently multi-modal nature of human paths which makes socially-acceptable multiple futures when human interactions are involved. To this end, we propose a new generative model for multi-future trajectory prediction based on Conditional Variational Recurrent Neural Networks (C-VRNNs). Conditioning relies on prior belief maps, representing most likely moving directions and forcing the model to consider the collective agents' motion. Human interactions are modeled in a structured way with a graph attention mechanism, providing an online attentive hidden state refinement of the recurrent estimation. Compared to sequence-to-sequence methods, our model operates step-by-step, generating more refined and accurate predictions. To corroborate our model, we perform extensive experiments on publicly-available datasets (ETH, UCY and Stanford Drone Dataset) and demonstrate its effectiveness compared to state-of-the-art methods.

Keywords: trajectory forecasting, multi-future prediction, time series, variational recurrent neural networks, graph attention networks

1 Introduction

Trajectory forecasting has recently experienced exponential growth in several research areas such as video-surveillance, sports analytics, self-driving cars and physical systems [1]. More specifically, it can be useful for predicting pedestrians dynamics [2,3,4,5,6,7] and vehicles behaviour [8,9,10,11], as well as to understand the intentions of people and cars along the streets to avoid possible crashes. In sports analytics [12,13,14,15,16,17], being able to predict players trajectories can improve the action interpretation of each player during a match, while in physical systems it can be fundamental to predict particles dynamics in complex domains [18,19,20].

In this paper, we focus on pedestrian trajectory prediction in crowded areas which is a challenging task, especially in an interactive and multi-modal setting. Here two different strategies are commonly employed to model human

interactions: *pooling-based* and *graph-based* methods. Pooling-based methods [3,4,5,21,22,23] employ sequence-to-sequence models composed of an encoder to extract features from the observed trajectory, and a decoder to generate the subsequent time-steps, interspersed with pooling layers modeling interactions between neighbours. By contrast, graph-based methods [6,7,9,13,15,24,25] apply graph neural networks to model interactions; to this end, they generate each trajectory using recurrent encoder-decoder architectures and acting on different components of the recurrent network, such as hidden or internal states. Although these approaches have proven to be effective, some problems are still open, such as modeling long-term predictions and capturing subtle interactions among people in the foreseen future. Graph-based methods represent the most promising approaches [6,13,26] since they allow the model to consider not only the individual trajectory evolution but also to push jointly agents' predictions toward the future one time-step at a time; hence showing more robustness for long-term sequences. Many works have been proposed to take into account the inherently multi-modal nature of human trajectories [5,10,11,25,27]. Nevertheless, they scarcely investigate the main reasons pedestrians may choose different paths without jointly considering their past knowledge and interactions with other agents. Another relevant problem in trajectory prediction tasks is to consider scene constraints such as walls and other fixed obstacles in order to predict realistic paths. A common approach to overcome this issue is to introduce visual elements into the network such as images or semantic segmentation [22,26,28], but this implies the availability of the video stream both at train and test time.

In this work, we propose a novel method for multi-future trajectory forecasting that works in a completely generative setting, enabling the prediction of multiple possible futures. At each m time-step, it is possible to generate n samples, leading to predict n^m different paths. During online inference, we integrate human interactions at time-step level, allowing for other agents to affect the whole trajectory generation process. As a consequence, online interactions computation improves the predicted trajectories as the number of time-steps increases; hence containing the error growth. Technically, our model is a Conditional-VRNN, conditioned by prior belief maps on pedestrians frequent paths, that predicts future positions one time-step at a time, by relying on recurrent network hidden states.

The contributions of this paper are twofold:

- (i) We propose a new method to integrate human interactions into the model in an online fashion, basing on an hidden state refinement with a graph attentive mechanism. We employ a similarity-based adjacency matrix to take into account the neighbourhood.
- (ii) We introduce local belief maps to encourage the model to follow a prior transition distribution whenever the prediction is uncertain and to discourage unnatural behaviour such as crossing obstacles, avoiding to employ additional visual inputs. Such behaviour is imposed during training by a KL divergence loss between ground-truth and samples contributing to the model performances refinement.

Our model achieves state-of-the-art performance on several standard benchmarks using different evaluation protocols. We also outperform both competitors and baselines on Stanford Drone Dataset (SDD) showing the robustness of our architecture to different urban contexts.

2 Related Work

Trajectory prediction can be approached as a time-series forecasting problem. The goal is to predict a portion of a sequence of data that evolves over time given a previously observed one. Traditionally, trajectory prediction has been approached with rule-based and social force models [2,29,30] that have been proven to be effective in simple contexts, but they fail to generalize to different domains. Only in the last few years, the multi-modal nature of trajectories has gained attention in future paths generation through the use of generative models [5,14,15,26]. However, the task requires to take into account not only the trajectory evolution over time but also how agents influence each other. Depending on how people interactions are handled, we group related work into position-based models, which uses only spatial information, and graph-based models, which rely on connected structures.

Position-based models. Social-LSTM [3] models individual trajectory as an LSTM encoder-decoder and considers interactions using a social pooling mechanism. This module handles human interactions fusing hidden states of pedestrians in the neighbourhood. Social GAN [5] uses a pooling mechanism in combination with a generative model to predict socially acceptable trajectories. Sophie [28] consists of a Generative Adversarial Network (GAN), which leverages the contribution of a social attention module and a physical attention module. The first one encodes the interactions using the path history of all the agents, while the second one accounts the scene context information through images. SS-LSTM [4] uses different inputs to also take into account the influence of the environment and maps of the neighbourhood to narrow the field of mutual influences.

Graph-based models. Graph Neural Networks (GNN) have been used to model interactions between different trajectories. Graph Variational RNNs [13] model multi-agent trajectory data mainly focusing on multi-player sports games. Each agent is represented by a VRNN where prior, encoder and decoder are modeled as message passing GNNs allowing agents to weakly share information through nodes. Neural Relation Inference (NRI) [18] learns to infer interactions with two-steps message passing methods concurrently learning the dynamics from observed data in an unsupervised fashion. Graph-structured variational recurrent neural network [15], based on relation networks, infers the current state and forecasts future states of basket and football players trajectories. SR-LSTM [7] uses a state refinement module through a motion gate and pedestrian-wise attention. Social-BiGAT [26] presents a graph-based generative adversarial

network based on GAT [31] that learns reliable future representations that encode the social interactions between humans in the scene and contextual images to incorporate scene information. A recurrent encoder-decoder architecture is trained adversarially to predict paths. STGAT [6] proposes a model based on two levels of LSTMs to incorporate interactions through a hidden state refinement based on GAT during the encoding part, while the decoder generates future positions. A generative hierarchical structure of macro-intents [14], obtained via labelling functions, learns low-dimensional representations of data that extend both in time and space for multiple coordinating players in basketball game. Macro-intents are labelled with programmatic weak supervision, computing the region of the court in which players remain stationary. VRNN with an intermediate layer is used to model macro-intents.

In contrast to approaches based on Variational Autoencoder (VAE) [13,15,18], our method does not model the entire prediction as a graph, but uses an attentive module to refine the hidden state of the recurrent network. In this way, it is possible to refine the past history of a single pedestrian with information about the history of other agents. Unlike sports games, where each agent can influence all other agents, in urban settings neighbourhood information is crucial since the influence on pedestrians may depend on their mutual distance. Our model resembles [7] and [6] that combine LSTMs and GNNs. Nevertheless, SR-LSTM [7] works on the cell state of the LSTM considering current interactions instead of their history. However, our intuition is that, in sequence prediction tasks, past interactions heavily influence the future. STGAT [6] uses GAT as hidden state refinement, but it uses a sequence-to-sequence model, so the predicted interactions are based on the observed ones, without an online refinement. Both methods do not take into account contextual information (e.g. belief maps) or collective behaviors in order to avoid the prediction of unnatural paths.

3 AC-VRNN Model

Pedestrian dynamics are primarily affected by neighbourhood space in urban areas. To avoid obstacles or other people, pedestrians continuously steer their motion also gaining the advantage of prior knowledge acquired in similar contexts. To this end, our model relies on the past motion of monitored scenes as well as structured interactions in a generative setting.

Problem formulation. Given a pedestrian at time-step t , his/her current position is represented by 2-D coordinates. Our model analyzes a temporal window of T_{obs} time-steps to predict motion dynamics during the next T_{pred} time-steps. Similarly to [5], our model uses displacements with respect to the previous points. More specifically, given a sequence of displacements $(\Delta x_0, \dots, \Delta x_{T_{pred}})$, we observe a part of the sequence $(\Delta x_0, \dots, \Delta x_{T_{obs}})$ and predict the subsequent one $(\Delta x_{T_{obs}+1}, \dots, \Delta x_{T_{pred}})$. In the following, we use \mathbf{x}_t and Δx_t interchangeably to denote a displacement at time t .

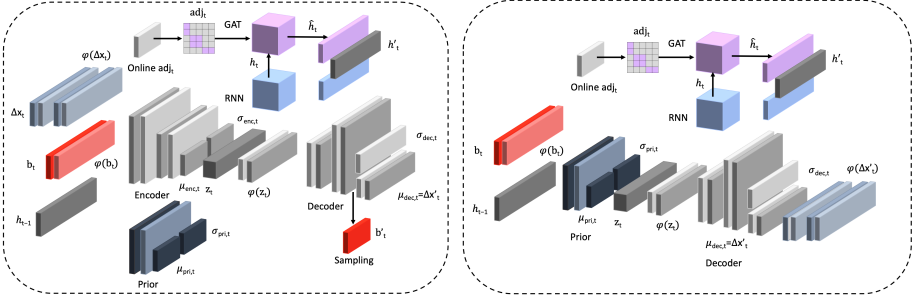


Fig. 1: Proposed trajectory prediction framework for a single time-step. The overall model is composed of a training module (left) and an inference module (right). The former is composed of a recurrent variational autoencoder conditioned on prior belief maps. The hidden state of the RNN is refined with an attentive module for the next step of recurrence. The latter performs the displacements generation through the prior network on \mathbf{h}_t and makes an online computation of the adjacency matrix which defines connections between pairs of nodes.

Our Attentive Conditional Variational Recurrent Neural Network (AC-VRNN), shown in Fig. 1, is composed of three building blocks:

- (i) a VRNN to generate sequence of displacements in a multi-modal way;
- (ii) a hidden state refinement based on an attentive mechanism to model the interactions within the neighbourhood, performed at a time-step level during training and inference phases;
- (iii) a belief map to encourage the model to follow the prior belief when the model is uncertain, thus avoiding to predict samples that may fall within never crossed areas.

3.1 Predictive VRNN

Variational Recurrent Neural Networks (VRNNs) [32] explicitly model dependencies between latent random variables \mathbf{z}_t across subsequent time-steps. VRNNs contain a Variational Autoencoder (VAE) [33] at each time-step conditioned on the hidden state variable \mathbf{h}_{t-1} of a RNN to take into account the temporal structure of sequential data. At each time-step, prior, encoder and decoder output multivariate normal distributions, with three functions f_{pri} , f_{enc} and f_{dec} modeling their means and variances.

Similarly to VAEs, the true posterior is intractable, so it is approximated by a neural network q_ϕ , which also depends on the hidden state \mathbf{h}_{t-1} under

recurrency equations:

$$p_{\theta}(\mathbf{z}_t | \mathbf{x}_{<t}, \mathbf{z}_{<t}) = \mathcal{N}\left(\mathbf{z}_t | \boldsymbol{\mu}_{\text{pri},t}, (\boldsymbol{\sigma}_{\text{pri},t})^2\right), \quad (\text{prior}) \quad (1)$$

$$q_{\phi}(\mathbf{z}_t | \mathbf{x}_{\leq t}, \mathbf{z}_{<t}) = \mathcal{N}\left(\mathbf{z}_t | \boldsymbol{\mu}_{\text{enc},t}, (\boldsymbol{\sigma}_{\text{enc},t})^2\right), \quad (\text{inference}) \quad (2)$$

$$p_{\theta}(\mathbf{x}_t | \mathbf{x}_{<t}, \mathbf{z}_{\leq t}) = \mathcal{N}\left(\mathbf{x}_t | \boldsymbol{\mu}_{\text{dec},t}, (\boldsymbol{\sigma}_{\text{dec},t})^2\right), \quad (\text{generation}) \quad (3)$$

$$\mathbf{h}_t = f_{\text{rnn}}(\mathbf{x}_t, \mathbf{z}_t, \mathbf{h}_{t-1}). \quad (\text{recurrence}) \quad (4)$$

These functions can be deep neural networks with learnable parameters θ and ϕ that output $(\boldsymbol{\mu}_{\text{pri},t}, \boldsymbol{\sigma}_{\text{pri},t})$, $(\boldsymbol{\mu}_{\text{enc},t}, \boldsymbol{\sigma}_{\text{enc},t})$ and $(\boldsymbol{\mu}_{\text{dec},t}, \boldsymbol{\sigma}_{\text{dec},t})$, respectively. The generative and inference processes are jointly optimized by maximizing the following variational lower bound (ELBO) with respect to their parameters:

$$ELBO = \mathbb{E}_{q_{\phi,t}(\mathbf{z}_t)} \left[\sum_{t=1}^T (-\text{KL}(q_{\phi,t}(\mathbf{z}_t) \| p_{\theta,t}(\mathbf{z}_t)) + \log p_{\theta,t}(\mathbf{x}_t)) \right], \quad (5)$$

where KL represents the KullbackLeibler divergence (where we omit the conditioning variables to keep the notation light).

We use VRNN in a predictive setting. In this context, there is not a real distinction between observations and predictions. VRNN learns at each time-step to generate the current displacement, given the input and the hidden state of the RNN. At inference time, the model only uses the last hidden state from the observed sequence, then generates the subsequent time-steps. Differently from all other trajectory prediction models, AC-VRNN is a generative model used in a predictive setting. This way, it generates one displacement at a time and it is simple to incorporate the interactions at time-step level, without the need of leveraging observations in a single encoding.

3.2 Attentive Hidden State Refinement

Pedestrians dynamics are mainly influenced by surrounding agents. Our model handles human interactions using an attentive hidden state refinement of the RNN through a graph neural network, as shown in Fig. 2(a).

The hidden state refinement resembles the idea proposed by GAT [31] which adopts an attention mechanism to learn relative weights between two connected nodes, through specific transformations called graph attentional layers. At time-step t , our refinement strategy considers a set of hidden state nodes $\{\mathbf{h}_t^1, \dots, \mathbf{h}_t^N\}$, where each $\mathbf{h}_t^i \in \mathbb{R}^F$ represents the hidden state of the i -th agent in the scene. The attention layer produces a new set of node features $\{\hat{\mathbf{h}}_t^1, \dots, \hat{\mathbf{h}}_t^N\}$, $\hat{\mathbf{h}}_t^i \in \mathbb{R}^{F'}$ as its output. The transformation is parametrized by a weight matrix $\mathbf{W} \in \mathbb{R}^{F' \times F}$ (shared between graph nodes) and a weight vector $\mathbf{a} \in \mathbb{R}^{2F'}$. Self-attention coefficients $\alpha_{i,j}$ between the nodes \mathbf{h}_t^i and \mathbf{h}_t^j are computed as follows:

$$\alpha_{i,j} = \frac{\exp\left(\text{LeakyReLU}\left(\mathbf{a}^T \left[\mathbf{W}\mathbf{h}_t^i \| \mathbf{W}\mathbf{h}_t^j\right]\right)\right)}{\sum_{k \in \mathcal{N}_i} \exp\left(\text{LeakyReLU}\left(\mathbf{a}^T \left[\mathbf{W}\mathbf{h}_t^i \| \mathbf{W}\mathbf{h}_t^k\right]\right)\right)}, \quad (6)$$

where \parallel represents the concatenation operator. The normalized attention coefficients are used to compute a linear combination of the features which represents the final output feature for every node, followed by a ELU non-linearity [34] acting on the neighbourhood \mathcal{N}_i of the i -th node:

$$\hat{\mathbf{h}}_t^i = \text{ELU} \left(\sum_{j \in \mathcal{N}_i} \alpha_{i,j} \mathbf{W} \mathbf{h}_t^j \right). \quad (7)$$

The neighbourhood \mathcal{N}_i defines the set of nodes with positive adjacency with respect to the i -th agent. The adjacency matrix follows a similarity-based principle, and it is computed, inspired by proxemics interaction theory [35], considering the heat kernel of the distance $d(i, j)$ between each pedestrian, $\exp \left(-\frac{d(i,j)}{2\sigma^2} \right)$, where σ is a smoothing hyperparameter. During training, the VRNN takes as input a batch of sequences corresponding to considered time-steps. At each time-step t , it computes and samples the next position \mathbf{x}_t^i for each pedestrian i . Then, the graph attention mechanism acts on the hidden state \mathbf{h}_t^i (provided by Eq. (4)) to compute the corresponding interaction-refined state $\hat{\mathbf{h}}_t^i$. The refined hidden state $\hat{\mathbf{h}}_t^i$ is concatenated to the original one and a final linear projection is applied as follows:

$$\mathbf{h}_t'^i = \text{Linear} \left(\mathbf{h}_t^i \parallel \hat{\mathbf{h}}_t^i \right). \quad (8)$$

At the next time-step, the VRNN takes as input the above hidden state $\mathbf{h}_t'^i$ which carries information about interactions of previous time-steps.

3.3 Conditional-VRNN on Belief Maps

Being a stochastic model, our AC-VRNN could eventually exhibit high predictive variance hence generating predictions far from expected ones. To balance the bias/variance trade-off of the predictor, we introduce belief maps on displacements. These maps contain information about the collective behavior of each agent in the scene, leading the model to partially follow this behavior. In this way, the model is discouraged to predict displacements close to never-crossed areas, avoiding the generation of non-realistic paths.

Belief Maps. Belief maps are computed dividing the coordinate space for each scene into a $N \times M$ grid. The boundaries of the global grid are given by minimum and maximum coordinates along x and y directions. The values of N and M define the grid coarse and are computed considering the average displacement μ and its standard deviation σ as follows:

$$N = \left\lceil \frac{(x_{max} - x_{min})}{\frac{\mu + \sigma}{2}} \right\rceil, \quad M = \left\lceil \frac{(y_{max} - y_{min})}{\frac{\mu + \sigma}{2}} \right\rceil. \quad (9)$$

For each grid location (bin), a $L \times L$ neighbourhood is then considered (with $L = 5$). For each (x, y) location, we get the corresponding $L \times L$ neighbourhood

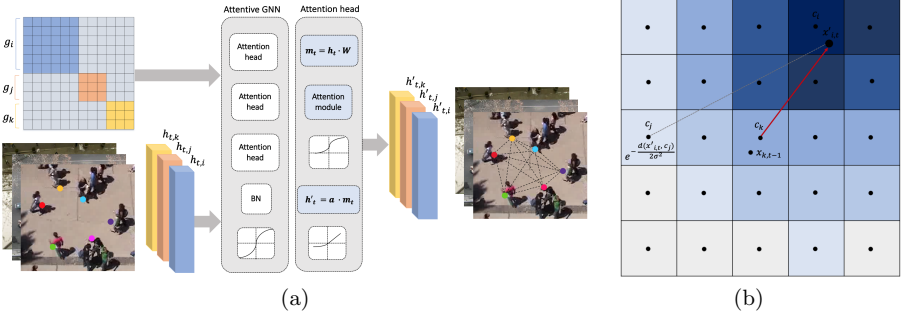


Fig. 2: Scheme of the proposed attentive hidden state refinement process. The adjacency matrix is an irregular block matrix where each block size is defined by the number of pedestrians in the current scene (a). Belief map during training for one sample using heat similarity-based strategy. The map is centred at $t - 1$ to display the sampled displacements distribution at t (b).

and compute the heat kernels between the next location and the neighbourhood bins centres⁴. This procedure is repeated for all the trajectories and bins values are accumulated by summation. Each belief map \mathbf{b} , i.e. a $L \times L$ sub-grid indexed by the (x, y) location in the scene, is subsequently normalized in order to transform the cumulative grid into a probability distribution.

Unlike the recurrent process within the VRNN, the creation of belief maps is a Markov process, as their generation only depends on single-step transitions.

Conditional-VRNN. We exploit the belief maps to encourage the model to follow the average behaviour shown by previously observed agents. A conditional version of VAE is proposed by [36] and [37], whereas [38] propose a conditional-flow variational autoencoder for structured prediction on time series. In our work, we use a recurrent version of [36], conditioning VRNN on belief maps. At each time-step, *prior*, *encoder* and *decoder* networks take the belief map at $t - 1$ as input, conditioning the resultant Gaussian distribution. We embed belief maps with a linear projection before feeding them into the VRNN blocks.

$$\mu_{\text{pri},t}, \sigma_{\text{pri},t} = f_{\text{pri}}(\mathbf{h}_{t-1}, \mathbf{b}_{t-1}; \theta) \quad (10)$$

$$\mu_{\text{enc},t}, \sigma_{\text{enc},t} = f_{\text{enc}}(\mathbf{x}_t, \mathbf{h}_{t-1}, \mathbf{b}_{t-1}; \phi) \quad (11)$$

$$\mu_{\text{dec},t}, \sigma_{\text{dec},t} = f_{\text{dec}}(\mathbf{z}_t, \mathbf{h}_{t-1}, \mathbf{b}_{t-1}; \theta) \quad (12)$$

KL Divergence. In addition to conditioning the model on belief maps, a further loss term is inserted, in order to optimize the affinity between ground-truth maps and those generated by the model. By sampling multiple displacements

⁴ The proposed course of the global grid and a 5×5 belief map guarantee that most of subsequent displacements fall into the corresponding belief map.

from the model, we obtain the sampled candidate belief map \mathbf{s}_{t-1} , which identifies a probability distribution over local bin transitions. For each sampled displacement and the consequent location, we index the corresponding grid bin, then the heat kernel value between the sampled next location and the $L \times L$ neighbourhood bin centres is used to fill the grid continuously (see Fig. 2(b)). The aforementioned procedure allows to unroll the sub-grids, obtaining for every location a discrete probability density of possible transitions. Thus, it is possible to compare generated belief maps \mathbf{s}_{t-1} and ground-truth ones \mathbf{b}_{t-1} by means of the KL divergence, exploiting the histogram loss term in [39]. We add this contribution to the ELBO loss in Eq. (5) encouraging the model to be compliant to the collective behaviour of all agents. Such a divergence measure is multiplied by a constant k for loss balancing to ensure that it has a weight comparable with the other loss components:

$$L = \mathbb{E}_{q_{\phi,t}(\mathbf{z}_t)} \left[\sum_{t=1}^T (-\text{KL}(q_{\phi,t}(\mathbf{z}_t) \| p_{\theta,t}(\mathbf{z}_t)) + \log p_{\theta,t}(\mathbf{x}_t) + k \text{KL}(\mathbf{b}_{t-1} \| \mathbf{s}_{t-1})) \right]. \quad (13)$$

4 Experiments

4.1 Datasets

We present experiments on different datasets to prove the robustness of our model on different scenarios and protocols. In particular, we define three experiments with increasing degree of interactions complexity: ETH [40], UCY [41] and Stanford Drone Dataset [42].

We compare our model with the most recent works on trajectory prediction achieving state-of-the-art results on several scenes.

ETH-UCY. ETH [40] and UCY [41] are two standard datasets in the context of trajectory prediction. ETH consists of two scenes, *Eth* and *Hotel*, while UCY consists of three scenes, *Zara1*, *Zara2* and *Univ*. The benchmark contains different type of interactions between pedestrians and fixed obstacles such as buildings or parked cars.

Stanford Drone Dataset. SDD [42] is a more recent large scale dataset, containing urban scenes of a university campus, streets and intersections, shot by a drone. It collects images, videos and annotations of various types of agents such as pedestrians, bicyclists, skateboarders, cars, buses, and golf carts. More specifically, it is composed of 31 videos of 8 different scenarios. This dataset provides more complex scenes, involving various type of human interactions. We use the version proposed by TrajNet benchmark [43,44] which contains only pedestrian annotations. We split the training set of SDD World Plane Human-Human dataset into three sets for the learning process. For each scene, we select 70% of data as train set, 10% as validation set and the remaining part as test set. Finally, we create three unique sets for training, validating and testing.

4.2 Metrics

In a predictive setting, we can evaluate the discrepancy between ground-truth and predicted trajectories. To quantitatively evaluate our models, we consider the following metrics:

- **Average Displacement Error (ADE)**: Average Euclidean distance over all estimated points and ground-truth positions of a trajectory as proposed in [40]:

$$ADE = \sum_{i=1}^{\mathcal{P}} \sum_{t=T_{obs}+1}^{T_{pred}} \frac{\sqrt{(\hat{x}_t^i - x_t^i)^2 + (\hat{y}_t^i - y_t^i)^2}}{T_{pred} \cdot \mathcal{P}}; \quad (14)$$

- **Final Displacement Error (FDE)**: Average Euclidean distance between predicted and ground-truth final destinations:

$$FDE = \sum_{j=1}^{\mathcal{P}} \frac{\sqrt{(\hat{x}_{T_{pred}}^j - x_{T_{pred}}^j)^2 + (\hat{y}_{T_{pred}}^j - y_{T_{pred}}^j)^2}}{\mathcal{P}}; \quad (15)$$

where \mathcal{P} represents the number of pedestrians and T_{pred} is the predicted time horizon.

4.3 Comparison with State-Of-The-Art Methods

ETH-UCY datasets. Due to different versions and training protocols proposed by different competitive methods on ETH and UCY datasets, we test our model on three versions of the datasets to equally compare AC-VRNN with our baselines. Quantitative results are reported in Table 1. We indicate as AC-VRNN our complete model and as A-VRNN our model without employing belief maps. Firstly, we consider a leave-one-out training protocol as in S-GAN [5] (A). Our model outperforms all baselines on *Zara2* scene and exhibits the best values on average metrics. We achieve the best performance with A-VRNN, on both ADE and FDE. Slightly worst performance of AC-VRNN could be ascribed to the leave-one-out protocol since training belief maps may not comply with test scenes increasing uncertainty for future predictions. SR-LSTM [7] defines a different *Eth* annotations considering 6 frames at 0.4s instead of 10 frames due to a frame rate issue of the original annotations, affecting each cross-validation fold (B). In this case, our model outperforms SR-LSTM baseline or achieve comparable results on all datasets for both metrics. Finally, S-Ways [21] does not use leave-one-out protocol. Each dataset is split into 5 subsets, using 4 subsets for training and the remaining for testing purpose (C). We achieve better performance on ADE and slightly worse performance on FDE. Without the leave-one-out protocol, AC-VRNN significantly outperforms A-VRNN on FDE suggesting the beneficial effect of belief maps conditioning.

Table 1: Quantitative results of all methods across ETH and UCY datasets. We report two error metrics Average Displacement Error (ADE) and Final Displacement Error (FDE) for $t_{obs} = 8$ and $t_{pred} = 12$ in meters. The first block of experiments is relative to S-GAN and STGAT version of the dataset (i.e., leave-one-out protocol), the second is relative to SR-LSTM version, while the last experiments are trained with S-Ways protocol.

Method	ETH	HOTEL	UNIV	ZARA1	ZARA2	AVG
S-LSTM [3]	1.09/2.35	0.79/1.76	0.67/1.40	0.47/1.00	0.56/1.17	0.72/1.54
S-GAN-P [5]	0.87/1.62	0.67/1.37	0.76/1.52	0.35/0.68	0.42/0.84	0.61/1.21
S-GAN [5]	0.81/1.52	0.72/1.61	0.60/1.26	0.34/0.69	0.42/0.84	0.58/1.18
SoPhie [28]	0.70/1.43	0.76/1.67	0.54/1.24	0.30 /0.63	0.38/0.78	0.54/1.15
(A) Social-BiGAT [26]	0.69/ 1.29	0.49/1.01	0.55/1.32	0.30 / 0.62	0.36/0.75	0.48/1.00
Next [22]	0.73/1.65	0.30 /0.59	0.60/1.27	0.38/0.81	0.31/0.68	0.46/1.00
STGAT [6]	0.78/1.60	0.30 / 0.54	0.51 / 1.08	0.33/0.72	0.29/0.63	0.44 /0.91
A-VRNN (Our)	0.73/1.45	0.34/0.65	0.53/1.14	0.33/0.69	0.26 / 0.54	0.44 / 0.89
AC-VRNN (Our)	0.68 /1.34	0.35/0.69	0.58/1.22	0.34/0.68	0.28/0.59	0.45/0.90
(B) SR-LSTM [7]	0.63/1.25	0.37 / 0.74	0.51 / 1.10	0.41/0.90	0.32/0.70	0.45/0.94
A-VRNN (Our)	0.60 / 1.18	0.37 / 0.74	0.55/1.20	0.39 / 0.83	0.27 / 0.59	0.44 / 0.91
(C) S-Ways [21]	0.39 / 0.64	0.39/0.66	0.55 / 1.31	0.44/ 0.64	0.51/0.92	0.46/ 0.83
A-VRNN (Our)	0.60/1.24	0.22/0.45	0.61/1.34	0.46/1.06	0.30 / 0.67	0.44 /0.95
AC-VRNN (Our)	0.55/1.06	0.18 / 0.26	0.76/1.59	0.37 /0.72	0.33/0.70	0.44 /0.87

Stanford Drone Dataset. To consider more complex urban scenarios, we test our model also on Stanford Drone Dataset. We compare our results with S-GAN-P [5] and STGAT [6]. As shown in Table 2, AC-VRNN outperforms A-VRNN version and both selected baselines. With more complex trajectories and scene topologies, our attentive module is more able to capture interactions between pedestrians and belief maps help to avoid incorrect behavior following the prior distribution of displacements in the scene.

To better evaluate our model performance, we also compute mean squared errors and their discrete derivatives at each prediction step. They are computed as follows:

$$L_2 = \sum_{i=1}^{\mathcal{P}} \frac{(\hat{x}_t^i - x_t^i)^2 + (\hat{y}_t^i - y_t^i)^2}{\mathcal{P}}, \quad \frac{dL_2}{dt} = \frac{L_{2,t} - L_{2,t-1}}{\Delta t}. \quad (16)$$

Such metrics highlight the increase of the error over time and provide information on possible trends for longer sequences. We compare our model with S-GAN-P [5] and STGAT [6]. Results reported in Fig. 3 show that both L2-error and its derivative on AC-VRNN increase slowly with respect to other methods, exhibiting promising results for long-term sequence prediction.

Table 2: ADE and FDE for $t_{obs} = 8$ and $t_{pred} = 12$ in meters on Stanford Drone Dataset.

Method	SDD
S-GAN-P[5]	0.65/1.26
STGAT[6]	0.57/1.09
A-VRNN (Our)	0.56/1.14
AC-VRNN (Our)	0.56/1.02

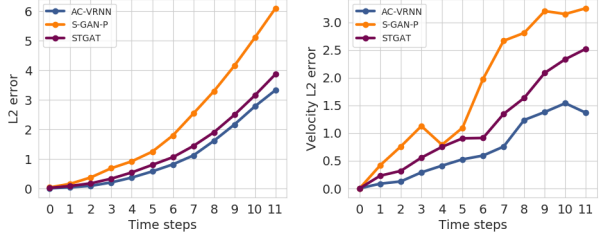


Fig. 3: L2 error (left) and velocity of the L2 error (right) at each predicted time-step on Stanford Drone Dataset.

4.4 Ablation Experiments

We also present an ablation study to show the contribution of different components of our model on the prediction task. In the following, we detail each component and report quantitative results in Table 3.

Vanilla Variational Recurrent Network. We investigate the ability of Vanilla VRNNs to predict accurate trajectories on ETH, UCY and SDD datasets. Such model does not consider any human interactions or prior scene knowledge. ETH scenes appear mainly affected by the lack of additional information while UCY scenes attains comparable results to our AC-VRNN model, especially for ADE metric. Such a result highlights the importance of trajectory forecasting task to go beyond a time-series problem and the need to include contextual information about the scene, such as human interactions or experience gained in similar contexts.

Hidden State Refinement with Graph Convolutional Neural Network. This experiment models interactions with a hidden state refinement based on a standard Graph Convolutional Networks (GCN) [45]. The model has worse performance compared to AC-VRNN and Vanilla VRNN models on ETH and UCY datasets while obtains comparable results to AC-VRNN on SDD dataset. The experiments suggest that, for complex contexts, attention mechanism is able to capture more useful information to model interactions among pedestrians compared to simple scenes where interactions could be limited.

AC-VRNN without KLD Loss on Belief Maps. To demonstrate the importance of KL-divergence loss on belief maps, we train our model without this term while still conditioning the model on them. We obtain worst results on all datasets proving that the network is not able to integrate belief maps information only conditioning VAE components. KL-divergence leads the network to

Table 3: Ablation experiments showing ADE and FDE for $t_{obs} = 8$ and $t_{pred} = 12$ in meters on ETH, UCY and SDD datasets. AVG column reports average results for ETH and UCY datasets. We also report results of our A-VRNN and AC-VRNN models using the same protocol.

Method	ETH	HOTEL	UNIV	ZARA1	ZARA2	AVG	SDD
Vanilla VRNN	0.79/1.61	0.46/0.94	0.55/1.20	0.34/0.75	0.26/0.58	0.48/1.02	0.56/1.15
GCN-VRNN	0.81/1.58	0.41/0.85	0.59/1.31	0.38/0.84	0.41/0.96	0.52/1.11	0.53/1.05
AC-VRNN w/o KLD	0.73/1.41	0.52/1.07	0.64/1.36	0.43/0.89	0.39/0.83	0.54/1.11	0.60/1.11
All-1 ADJ Matrix	0.77/1.52	0.37/0.73	0.55/1.19	0.34/0.75	0.26/0.58	0.46/0.95	0.57/1.11
kNN ADJ Matrix	0.76/1.54	0.47/0.99	0.57/1.26	0.42/0.95	0.26/0.58	0.50/1.01	0.73/1.43
A-VRNN	0.73/1.45	0.34/0.65	0.53/1.14	0.33/0.69	0.26/0.54	0.44/0.89	0.56/1.14
AC-VRNN	0.68/1.34	0.35/0.69	0.58/1.22	0.34/0.68	0.28/0.59	0.45/0.90	0.56/1.02

generate displacement distributions similar to ground-truth ones and to follow prior knowledge about local behaviors.

Adjacency Matrix. We also evaluate our model using different kinds of adjacency matrices to corroborate the use of the similarity one.

All-1 Adjacency Matrix. We consider an *all-1* adjacency matrix where edges are equally weighted and all pedestrians in the scene are connected. This model achieves good performances but slightly worse than the ones obtained with similarity matrix on both ETH/UCY and SDD, proving that giving the same importance to all agents negatively affect the performances.

k-NN Adjacency Matrix. *k*-NN matrix only considers nearby pedestrians. The neighbourhood is computed by sorting mutual distances between each pedestrian, retaining only the first *k* nearest neighbours (with $k = 3$), defined as a set S_i . Each element is set to 1 if $a_{i,j} \in S_i$, to 0 otherwise.

k-NN matrix obtains quite worst results on ETH and UCY datasets and performs poorly on SDD dataset. This experiment demonstrates that a small neighbourhood is not able to capture interactions in large scenes where pedestrians show mutual influences also at long distance.

4.5 Qualitative Results

Fig. 4 presents some qualitative experiments, comparing our model with base-lines and competitive methods. On *Eth*, GCN-VRNN generates trajectories that significantly drift from the ground-truth ones. On *Zara1*, all considered models are able to follow correct paths, but AC-VRNN appears more able to predict complex trajectory such as the entrance into a building, following the collective agents' behaviour. On SDD *gates_0* and *deathCircle_0*, we show our model samples against competitive methods. All methods predict plausible paths, but

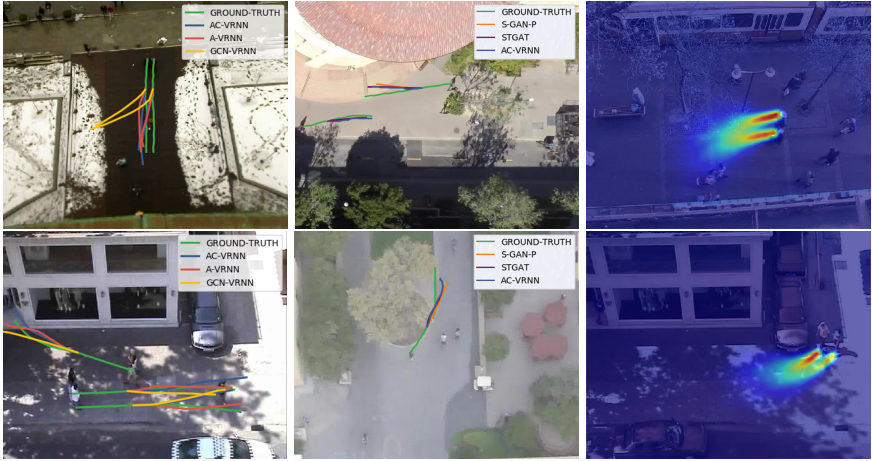


Fig. 4: Illustration of predicted trajectories using AC-VRNN, baselines and competitive methods on *Eth* and *Zara1* scenes of ETH and UCY datasets and *gates_0* and *death-Circle_1* of SDD. We also show heatmaps for two scenes generating a large number of samples.

AC-VRNN generates more realistic trajectories, following the sidewalk instead of crossing the road diagonally. Finally, we show heatmaps obtained generating a large number of samples to highlight the model ability to avoid collisions between two close pedestrians moving in the same direction. Since AC-VRNN is a completely generative model, it is possible to generate an unlimited number of future positions as well as creating trajectories without any observations. This could be particularly useful for applications that require sampling a large number of trajectories to simulate realistic motion dynamics as required by synthetic scenarios mimicking real-life situations. Obviously, as the number of time-steps increases, the predicted paths tend to drift from realistic ones, but our model qualitatively predicts plausible trajectories even after several time-steps. To this end, we show in Fig. 5 some qualitative experiments.

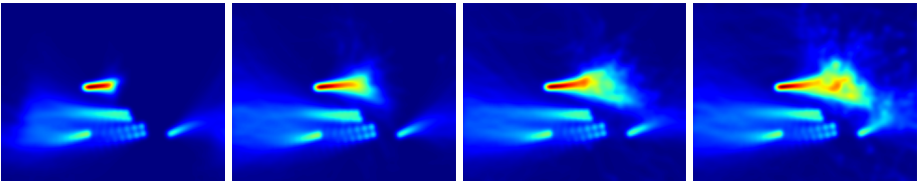


Fig. 5: Heatmaps representing long-term predictions for $t_{obs} = 8$ and $t_{pred} = 20, 60, 120$ and 200 , respectively (from left to right). We select *Zara1* scene and observe that the trajectories are coherent with the scene topology.

5 Conclusion

In this paper, we proposed a novel architecture for multi-future trajectory forecasting. Our framework uses VRNNs in a predictive setting. An attentive module includes interactions through a hidden state refinement based on a graph neural network in an on-line fashion at a time-step level. Finally, a local belief map encourages the model to follow a future displacement probability grid when the model is not confident about its prediction. We refer to our model as AC-VRNN and test it on several trajectory prediction datasets collected in different urban scenarios achieving best performance compared to state-of-the-art methods.

Our future work will be towards long-term predictions in order to deal with more complex and uncertain scenarios. Furthermore, an interesting aspect would be to include into the model additional scene context (e.g., depth data or WiFi/BLT signals) to design a multi-modal architecture.

References

1. Rudenko, A., Palmieri, L., Herman, M., Kitani, K.M., Gavrila, D.M., Arras, K.O.: Human motion trajectory prediction: A survey. ArXiv **abs/1905.06113** (2019)
2. Helbing, D., Molnar, P.: Social force model for pedestrian dynamics. *Physical review E* **51**(5) (1995) 4282
3. Alahi, A., Goel, K., Ramanathan, V., Robicquet, A., Fei-Fei, L., Savarese, S.: Social lstm: Human trajectory prediction in crowded spaces. In: 2016 IEEE Conference on Computer Vision and Pattern Recognition (CVPR). (June 2016) 961–971
4. Xue, H., Huynh, D.Q., Reynolds, M.: Ss-lstm: A hierarchical lstm model for pedestrian trajectory prediction. In: 2018 IEEE Winter Conference on Applications of Computer Vision (WACV). (March 2018) 1186–1194
5. Gupta, A., Johnson, J., Fei-Fei, L., Savarese, S., Alahi, A.: Social gan: Socially acceptable trajectories with generative adversarial networks. In: IEEE Conference on Computer Vision and Pattern Recognition (CVPR). (2018)
6. Yingfan, H., Huikun, B., Zhaoxin, L., Tianlu, M., Zhaoqi, W.: Stgat: Modeling spatial-temporal interactions for human trajectory prediction. In: The IEEE International Conference on Computer Vision (ICCV). (October 2019)
7. Zhang, P., Ouyang, W., Zhang, P., Xue, J., Zheng, N.: Sr-lstm: State refinement for lstm towards pedestrian trajectory prediction. In: IEEE Conference on Computer Vision and Pattern Recognition (CVPR). (2019)
8. Jiachen, L., Hengbo, M., Masayoshi, T.: Conditional generative neural system for probabilistic trajectory prediction. In: in 2019 IEEE/RSJ International Conference on Intelligent Robots and Systems (IROS), IEEE (2019)
9. Ma, Y., Zhu, X., Zhang, S., Yang, R., Wang, W., Manocha, D.: Trafficpredict: Trajectory prediction for heterogeneous traffic-agents. In: AAAI. (2018)
10. Charlie, Y., Tang, Ruslan, Salakhutdinov: Multiple futures prediction. In: nips. (2019)
11. Lee, N., Choi, W., Vernaza, P., Choy, C.B., Torr, P.H.S., Chandraker, M.K.: Desire: Distant future prediction in dynamic scenes with interacting agents. 2017 IEEE Conference on Computer Vision and Pattern Recognition (CVPR) (2017) 2165–2174
12. Felsen, P., Lucey, P., Ganguly, S.: Where will they go? predicting fine-grained adversarial multi-agent motion using conditional variational autoencoders. In: ECCV. (2018)
13. Raymond A., Y., Alexander G., Schwing, J.H., Kevin, M.: Diverse generation for multi-agent sports games. In: IEEE Conference on Computer Vision and Pattern Recognition (CVPR). (2019)
14. Zhan, E., Zheng, S., Yue, Y., Sha, L., Lucey, P.: Generating multi-agent trajectories using programmatic weak supervision. In: International Conference on Learning Representations (ICLR). (2019)
15. Sun, C., Karlsson, P., Wu, J., Tenenbaum, J.B., Murphy, K.: Stochastic prediction of multi-agent interactions from partial observations. In: International Conference on Learning Representations (ICLR). (2019)
16. Chieh-Yu, C., Wenze, L., Hsin-Ying, H., Wen-Hao, Z., Yu-Shuen, W., Jung-Hong, C.: Generating defensive plays in basketball games. In: Proceedings of the 26th ACM International Conference on Multimedia. MM '18, New York, NY, USA, ACM (2018) 1580–1588
17. Hsin-Ying, H., Chieh-Yu, C., Yu-Shuen, W., Chuang, J.H.: Basketballgan: Generating basketball play simulation through sketching. In: Proceedings of the 27th

- ACM International Conference on Multimedia. MM '19, New York, NY, USA, ACM (2019) 720–728
18. Kipf, T., Fetaya, E., Wang, K.C., Welling, M., Zemel, R.: Neural relational inference for interacting systems. arXiv preprint arXiv:1802.04687 (2018)
 19. Alet, F., Weng, E., Lozano-Pérez, T., Kaelbling, L.P.: Neural relational inference with fast modular meta-learning. In: NeurIPS 2019. (2019)
 20. Webb, E., Day, B., Andres-Terre, H., Lió, P.: Factorised neural relational inference for multi-interaction systems. In: ICML 2019 Workshop on Learning and Reasoning with Graph-Structured Representations. (2019)
 21. Javad, A., Jean-Bernard, H., Julien, P.: Social ways: Learning multi-modal distributions of pedestrian trajectories with gans. In: Proceedings of the IEEE Conference on Computer Vision and Pattern Recognition Workshops (CVPRW). (2019) 0–0
 22. Junwei, L., Lu, J., Juan, C.N., G., H.A., Li, F.F.: Peeking into the future: Predicting future person activities and locations in videos. In: The IEEE Conference on Computer Vision and Pattern Recognition (CVPR). (June 2019)
 23. Lisotto, M., Coscia, P., Ballan, L.: Social and scene-aware trajectory prediction in crowded spaces. ArXiv **abs/1909.08840** (2019)
 24. Vemula, A., Muelling, K., Oh, J.: Social attention: Modeling attention in human crowds. 2018 IEEE International Conference on Robotics and Automation (ICRA) (2017) 1–7
 25. Liang, J., Jiang, L., Murphy, K., Yu, T., Hauptmann, A.: The garden of forking paths: Towards multi-future trajectory prediction. ArXiv **abs/1912.06445** (2019)
 26. Kosaraju, V., Sadeghian, A.A., Martín-Martín, R., Reid, I.D., Rezaeifighi, S.H., Savarese, S.: Social-bigat: Multimodal trajectory forecasting using bicycle-gan and graph attention networks. In: IEEE Conference on Computer Vision and Pattern Recognition (CVPR). (2019)
 27. Jiachen*, L., Hengbo*, M., Masayoshi, T.: Interaction-aware multi-agent tracking and probabilistic behavior prediction via adversarial learning. In: in 2019 IEEE International Conference on Robotics and Automation (ICRA), IEEE (2019)
 28. Sadeghian, A., Kosaraju, V., Sadeghian, A., Hirose, N., Savarese, S.: Sophie: An attentive gan for predicting paths compliant to social and physical constraints. In: CVPR. (2018)
 29. Mehran, R., Oyama, A., Shah, M.: Abnormal crowd behavior detection using social force model. In: IEEE International Conference on Computer Vision and Pattern Recognition Workshops. (06 2009) 935–942
 30. Zanlungo, F., Ikeda, T., Kanda, T.: Social force model with explicit collision prediction. EPL (Europhysics Letters) **93**(6) (mar 2011) 68005
 31. Veličković, P., Cucurull, G., Casanova, A., Romero, A., Liò, P., Bengio, Y.: Graph attention networks. International Conference on Learning Representations (ICLR) (2018)
 32. Chung, J., Kastner, K., Dinh, L., Goel, K., Courville, A., Bengio, Y.: A recurrent latent variable model for sequential data. In: Proceedings of the 28th International Conference on Neural Information Processing Systems - Volume 2. NIPS'15, Cambridge, MA, USA, MIT Press (2015) 2980–2988
 33. Kingma, D.P., Welling, M.: Auto-encoding variational bayes. CoRR **abs/1312.6114** (2013)
 34. Clevert, D.A., Unterthiner, T., Hochreiter, S.: Fast and accurate deep network learning by exponential linear units (elus). In: International Conference on Learning Representations. (2016)

35. Rios-Martinez, J., Spalanzani, A., Laugier, C.: From proxemics theory to socially-aware navigation: A survey. *International Journal of Social Robotics* **7**(2) (2015) 137–153
36. Kingma, D.P., Rezende, D.J., Mohamed, S., Welling, M.: Semi-supervised learning with deep generative models. In: *Proceedings of the 27th International Conference on Neural Information Processing Systems - Volume 2. NIPS'14*, Cambridge, MA, USA, MIT Press (2014) 3581–3589
37. Sohn, K., Yan, X., Lee, H.: Learning structured output representation using deep conditional generative models. In: *Proceedings of the 28th International Conference on Neural Information Processing Systems - Volume 2. NIPS'15*, Cambridge, MA, USA, MIT Press (2015) 3483–3491
38. Bhattacharyya, A., Hanselmann, M., Fritz, M., Schiele, B., Straehle, C.N.: Conditional flow variational autoencoders for structured sequence prediction. *arXiv abs/1908.09008* (2019)
39. Ustinova, E., Lempitsky, V.: Learning deep embeddings with histogram loss. In: *Neural Information Processing Systems*. (2016)
40. Pellegrini, S., Ess, A., Schindler, K., van Gool, L.: You'll never walk alone: Modeling social behavior for multi-target tracking. In: *2009 IEEE 12th International Conference on Computer Vision (ICCV)*. (Sep. 2009) 261–268
41. Lerner, A., Chrysanthou, Y., Lischinski, D.: Crowds by example. *Computer Graphics Forum* **26**(3) (2007) 1186–1194
42. Robicquet, A., Sadeghian, A., Alahi, A., Savarese, S.: Learning social etiquette: Human trajectory understanding in crowded scenes. In: *ECCV*. (2016)
43. Sadeghian, A., Kosaraju, V., Gupta, A., Savarese, S., Alahi, A.: Trajnet: Towards a benchmark for human trajectory prediction. *arXiv preprint* (2018)
44. Becker, S., Hug, R., Hübner, W., Arens, M.: Red: A simple but effective baseline predictor for the trajnet benchmark. In: *ECCV Workshops*. (2018)
45. Kipf, T.N., Welling, M.: Semi-supervised classification with graph convolutional networks. *arXiv preprint arXiv:1609.02907* (2016)

Supplementary Material

A Implementation Details

We train our model for 500 epochs on all the datasets. The learning rate is set to 10^{-3} with Adam optimizer and a batch size of 16. We use a gradient clipping of 10. The RNN is a GRU network with 1 layer and hidden size equals to 64. The latent space dimension is set to 16. The Graph Attention Network uses 4 attention heads with a hidden size of 8. Each belief map during training is generated sampling 100 displacements.

A.1 Warm-up on VRNN KL-Divergence

VRNN is trained with the ELBO loss that is composed of two terms: Negative Log-Likelihood and KL-Divergence. To correctly balance these two terms, we use a warm-up method that increases the weight in the range $[0, 1]$ of the KL-Divergence up to N epochs (with $N = 50$). After this learning period, we fix the KL weight to 1. This technique privileges the reconstruction error during the early epochs, to teach the network first to generate in a correct way. Only later it teach the network to approach the *encoder* and the *prior* means and log-variances.

A.2 Hidden State Initialization

The hidden state initialization has a strong impact on the RNN training process. We try three different initialization approaches:

- *Zero initialization*: the simple zero-tensor initialization.
- *Learned initialization*: a linear layer is trained to learn a global good initialization.
- *Absolute coordinate initialization*: the tensor is initialized with the first absolute coordinates to give space information to the learning process that is based on displacements generation.

We experimentally notice that the *absolute coordinate initialization* has more impact on the recurrent process leading to a global performance improvement. We use this kind of initialization for all the experiments.

A.3 Block Irregular Adjacency Matrix

AC-VRNN is based on a single Variational Recurrent Neural Network with shared parameters. To jointly compute a unique adjacency matrix for each time-step, we build a block matrix where each block contains the matrix corresponding to a single scene, randomly chosen from the training dataset. Blocks can have different dimensions since a variable number of agents may be present in the scene. For this reason, the resulting matrix is a block irregular adjacency matrix.

B Belief Maps Generation Algorithm

Algorithm 1 Belief Maps Generation Algorithm

```

1: function BELIEF_MAPS_GENERATION(trajectories)
2:    $N, M, \delta_x, \delta_y \leftarrow \text{get\_grid\_coarse}(\text{trajectories})$ 
3:    $x_{\min}, y_{\min}, x_{\max}, y_{\max} \leftarrow \text{get\_min\_max}(\text{trajectories})$ 
4:    $\text{global\_grid} \leftarrow \text{make\_global\_grid}(x_{\min}, y_{\min}, N, M, \delta_x, \delta_y)$ 
5:   for all  $\text{bin} \in \text{global\_grid}$  do
6:      $\text{local\_maps} \leftarrow [0, \dots, 0]$ 
7:     for all  $\text{trajectory} \in \text{trajectories}$  do
8:        $\text{neighbour\_centres} \leftarrow \text{get\_neighbour\_centres}(\text{bin}, \delta_x, \delta_y)$ 
9:       for all  $\text{index}, \text{coord} \in \text{trajectory}$  do
10:        if  $\text{coord}_x \in [\text{bin}_x, \text{bin}_x + \delta_x]$  and  $\text{coord}_y \in [\text{bin}_y, \text{bin}_y + \delta_y]$  then
11:           $\text{next\_coord} \leftarrow \text{trajectory}[\text{index} + 1]$ 
12:           $\text{local\_map} \leftarrow \text{similarity\_matrix}(\text{next\_coord}, \text{neighbour\_centres}, \text{local\_map})$ 
13:        end if
14:      end for
15:    end for
16:     $\text{local\_map} \leftarrow \text{normalize}(\text{local\_map})$ 
17:     $\text{local\_maps} \leftarrow \text{insert}(\text{local\_map})$ 
18:  end for
19:  return  $\text{local\_maps}$ 
20: end function

21: function GET_GRID_COARSE(trajectories)
22:    $\mu_x, \mu_y \leftarrow \text{mean\_displacements}(\text{trajectories})$ 
23:    $\sigma_x, \sigma_y \leftarrow \text{standard\_deviation\_displacements}(\text{trajectories})$ 
24:    $x_{\min}, y_{\min}, x_{\max}, y_{\max} \leftarrow \text{get\_min\_max}(\text{trajectories})$ 
25:    $N \leftarrow \frac{x_{\max} - x_{\min}}{\frac{\mu_x + \sigma_x}{2}}; M \leftarrow \frac{y_{\max} - y_{\min}}{\frac{\mu_y + \sigma_y}{2}}$ 
26:    $\delta_x \leftarrow \frac{x_{\max} - x_{\min}}{N}; \delta_y \leftarrow \frac{y_{\max} - y_{\min}}{M}$ 
27:   return  $N, M, \delta_x, \delta_y$ 
28: end function

29: function SIMILARITY_MATRIX( $\text{next\_coord}, \text{neighbour\_centres}, \text{local\_map}$ )
30:   for all  $\text{index}, \text{centre} \in \text{neighbour\_centres}$  do
31:      $\text{local\_map}[\text{index}] \leftarrow \text{accumulate}(e^{-\sqrt{(\text{next\_coord}_x - \text{centre}_x)^2 + (\text{next\_coord}_y - \text{centre}_y)^2}})$ 
32:   end for
33:   return  $\text{local\_map}$ 
34: end function

```

C Qualitative Samples

We present other qualitative examples generated by AC-VRNN model and its variations (see Fig. 6). Furthermore, we sample each trajectory multiple times to demonstrate the ability of our model to predict multi-modal paths (see Fig. 7). Finally, we depict in Fig. 8 probability distributions of future paths.

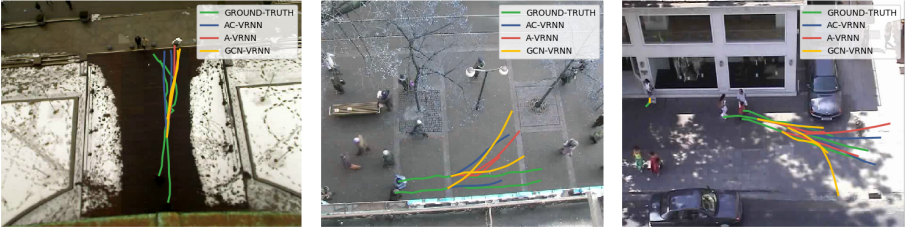


Fig. 6: Comparison between AC-VRNN prediction and baseline predictions.



Fig. 7: Multiple prediction of AC-VRNN trajectories to highlight the multi-modality nature of our model.

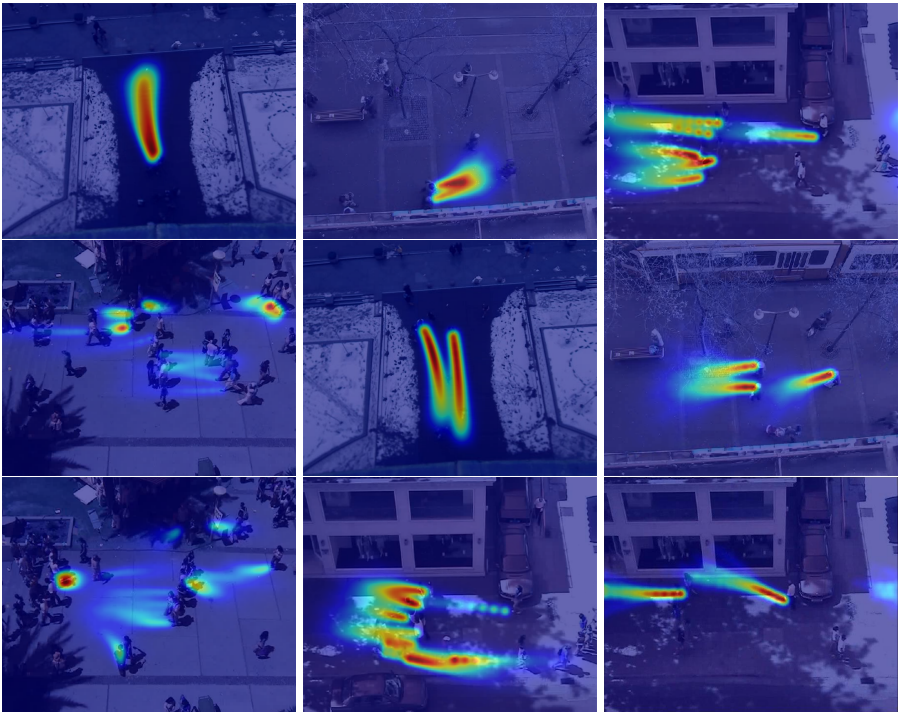


Fig. 8: Heatmaps representing probability distributions generated from N sampled trajectories on ETH and UCY dataset.